THE JOURNAL OF PHYSICAL CHEMISTRY C
A JOURNAL OF THE AMERICAN CHEMICAL SOCIETY

pubs.acs.org/JPCC

Article

Determining the Oblique Angle of Vertical Graphene Arrays Using Helicity-Resolved Raman Spectroscopy

Bo Xu, Shichen Xu, Yan Zhao, Shishu Zhang, Rui Feng, Jin Zhang, and Lianming Tong*

Cite This: J. Phys. Chem. C 2021, 125, 8353–8359

Read Online

ACCESS | Metrics & More | Article Recommendations | Supporting Information

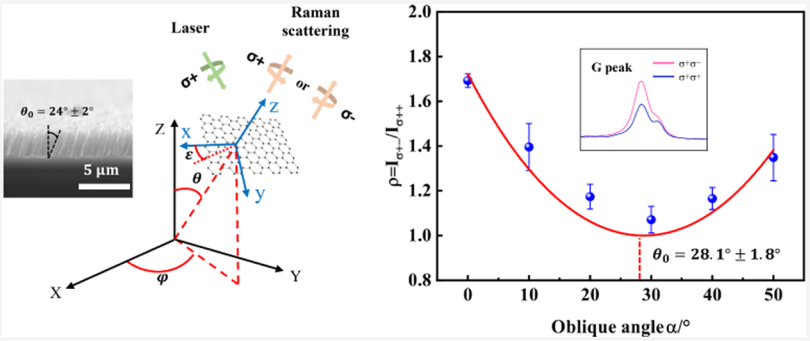

ABSTRACT: The microscopic structure of a macroscopic material assembled from a nanoscale determines its performance in practical functional applications. The rapid, effective, and in situ characterization of the microscopic structure, particularly the spatial orientation of nanomaterials in the assembly, is of urgent need but remains challenging. Herein, we report a Raman spectroscopic technique to characterize the oblique angle of vertical graphene (VG) arrays that are promising for thermal management applications. Raman spectroscopy is a powerful tool not only for the characterization of the composition and lattice structure of materials but also for the determination of structural orientation owing to the polarization-dependent Raman intensities. Using helicity-resolved Raman spectroscopy (HRRS), we show that the oblique angle of VG can be characterized quantitatively with an error of less than 5°. The technique is advantageous over the conventional linearly polarized Raman spectroscopy in simplicity and reliability, but if in combination, can be a versatile approach to characterize the spatial orientation of materials in more complex systems.

INTRODUCTION

Assemblies of nanomaterials have been explored extensively for various engineering applications.[1−5] For example, polymer nanocomposites reinforced by graphene or carbon nanotubes possess low mass density and exceptional mechanical properties and have been used as high-performance mechanical fibers.[6,7] Besides, vertical graphene (VG) arrays are a promising candidate for the next-generation thermal interface materials due to the high in-plane thermal conductivity of graphene.[8] The performance of these materials in practical functional applications is determined by the microscopic structures of the assemblies. If the fillers are aligned in the direction of strain for polymer nanocomposites, the reinforcement of mechanical performance, such as Young's modulus, can reach a maximum.[9] For carbon nanotube fibers, the elastic modulus is expected to be the highest if all nanotubes align parallel to the fiber.[10] VG arrays with flakes in consistent orientations have shown higher thermal conductivity than that with random orientations.[11] Numerous approaches have been used to design and control the microscopic structure of assemblies of nanomaterials or nanocomposites.[12−15] On the other hand, the characterization of the microscopic structures is of the same importance for understanding the relationship between the structure and performance. Several techniques have been used to characterize the microscopic structure including X-ray diffraction (XRD), transmission electron microscopy (TEM), and scanning electron microscopy (SEM).[15−18] However, it still remains a great challenge to develop in situ and rapid characterization techniques, from which the microscopic structures of materials in applied devices can be directly related to the performances.

Because of its fast, nondestructive, and time-efficient characterization, Raman spectroscopy stands as one of the most popular techniques in recent years. Not only can the composition, defects, and doping information be obtained from the Raman spectra,[19−21] but also can the Raman tensors

Received: March 3, 2021
Revised: March 21, 2021
Published: April 7, 2021

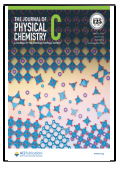

https://doi.org/10.1021/acs.jpcc.1c01937
J. Phys. Chem. C 2021, 125, 8353−8359

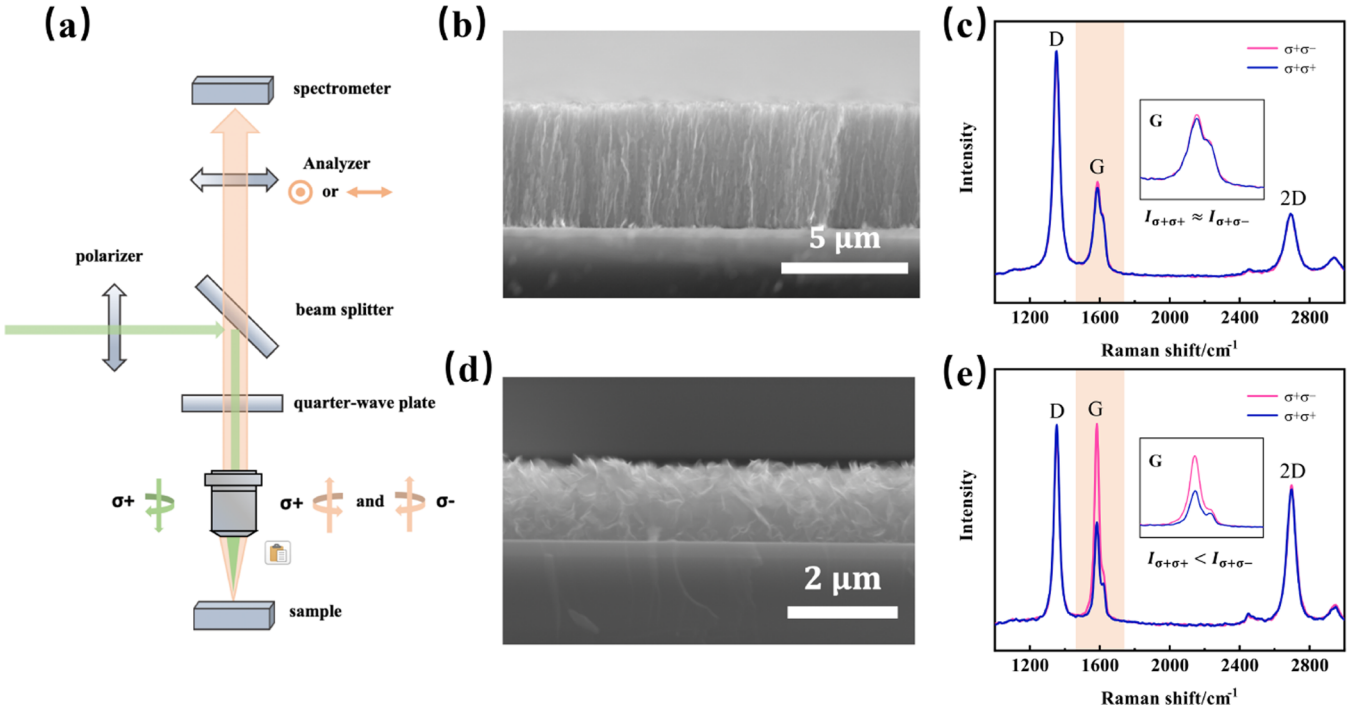

Figure 1. Helicity-resolved Raman scattering of VG arrays. (a) Schematic diagram of the experimental setup of helicity-resolved Raman spectroscopy. (b, c) The cross-sectional SEM image (b) of a VG array and corresponding helicity-resolved Raman spectra (c). (d, e) The cross-sectional SEM image (d) of a randomly oriented graphene array and corresponding helicity-resolved Raman spectra (e). The insets in (c) and (e) are the enlarged view of the G mode. The Raman spectra were normalized by the intensities of the 2D band. The wavelength of the excitation laser is 531.8 nm.

be measured from polarization-dependent Raman intensities.[22−26] In addition, the crystallographic orientation can be determined through polarized Raman scattering.[27−30] A series of studies have been reported on the determination of in-plane lattice orientation of two-dimensional (2D) materials, such as black phosphorus, and ReS_2 through angular-resolved Raman spectroscopy (ARPRS).[31−34] However, there has been no effective Raman spectroscopic approach to characterize the three-dimensional orientation distribution of nanomaterials in an assembly due to which the calculation of polarization-dependent intensities is complicated for linearly polarized Raman scattering in the backscattering configuration.

When excited by circularly polarized light, the Raman scattered light may also be circularly polarized. The helicity of the scattered light may be the same as or opposite to that of the incident light, which depends on the symmetry and spatial orientation of materials.[35,36] Helicity-resolved Raman spectroscopy (HRRS) refers to the selective detection of the helicity of Raman scattered light for circular polarization excitation. HRRS of 2D materials like graphene or transition metal dichalcogenides (TMDCs) have been studied systematically; for example, HRRS proves to be a powerful tool to resolve overlapping phonon modes and characterize excitonic nature as well as electron−phonon coupling for TMDCs.[36−40]

In this work, we develop an HRRS-based approach to quantitatively characterize the out-of-plane orientation (oblique angle) of VG arrays. First, we propose a theoretical model for HRRS intensity as a function of orientation angle for a graphene sheet, which indicates that the oblique angle of VG arrays can be measured through the intensity of the G mode with the same or opposite helicities. Our model is then confirmed by HRRS measurements of a VG array tilted by an angle from 0 to 60°, and the results are also compared with the randomly oriented graphene array. Finally, we apply this model to measure the oblique angle of an unknown sample with an error of less than 5°. In principle, if combined with ARPRS, our technique can be used to measure the three-dimensional spatial orientation in more complex systems.

EXPERIMENTAL SECTION

Preparation of VG Arrays. The VG arrays used in this work were grown by an alcohol-based electric-assisted plasma-enhanced chemical vapor deposition (AEF-PECVD) method onto Si/SiO_2 substrate according to ref 15. The experimental setup consists of an in-built electric field and conventional inductively coupled PECVD with a frequency of 13.56 MHz. VG arrays of different oblique angles were grown by placing substrates on quartz plates with certain angles. Randomly oriented graphene arrays were grown by the same PECVD system without an electric field.

Raman Measurement. Micro-Raman spectra were recorded using a JY Horiba HR800 Raman spectrometer in the backscattering geometry. The wavelengths of lasers used in this work are 531.8 nm (2.33 eV) and 632.8 nm (1.96 eV). The laser is focused on the sample by a 50× objective lens (NA = 0.5). The laser power is kept below 0.5 mW to avoid damage to samples.

RESULTS AND DISCUSSION

The experimental setup of helicity-resolved Raman spectroscopy is shown in Figure 1a. Left- or right-handed circularly polarized light is produced by a linear polarizer and the quarter-wave plate for incidence (helicity: σ_i). The Raman scattered light (helicity: σ_s) passes through the same quarter-

https://doi.org/10.1021/acs.jpcc.1c01937
J. Phys. Chem. C 2021, 125, 8353−8359

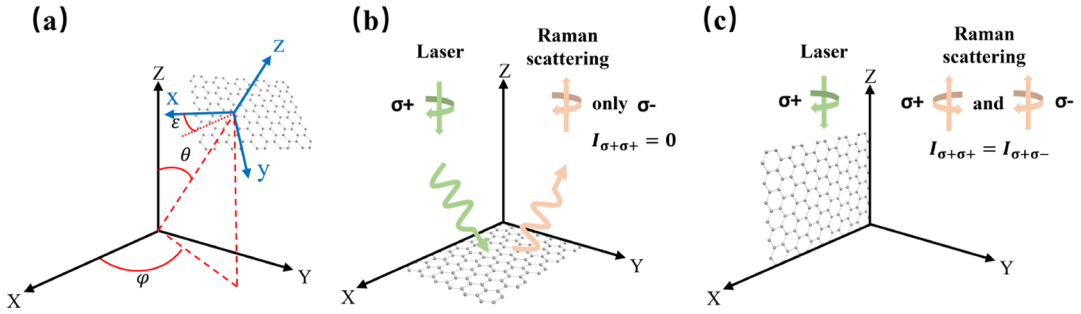

Figure 2. Schematic configurations for a graphene sheet with different orientations. (a) The presentation of Euler angles (θ,φ,ε) to express the three-dimensional orientation of a graphene sheet. θ is the nutation angle (out-of-plane orientation angle), φ is the precession angle (in-plane orientation angle), and ε is the rotation angle. (b, c) Schematic diagrams of the helicity selection rules for a horizontal (b) and vertical (c) graphene sheet.

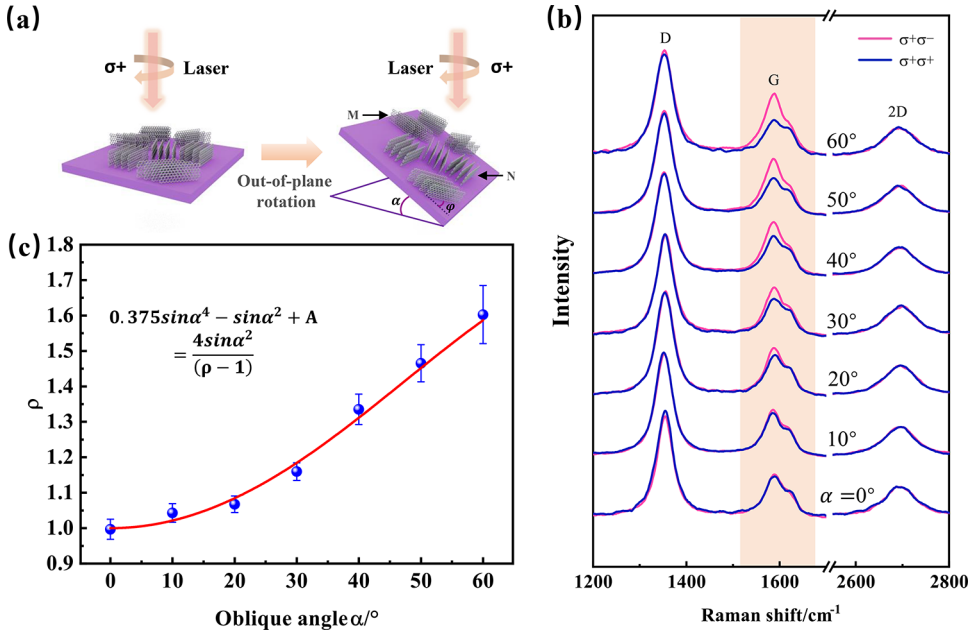

Figure 3. Quantitative characterization of a VG array with different tilting angles. (a) Schematic diagram of the VG array with a tilting angle α. (b) Helicity-resolved Raman spectra of the VG array with tilting angles from 0 to 60°. (c) Correlation of the polarization ratio ρ for the G mode with a tilting angle α. The Raman spectra were normalized by the intensities of the 2D band. The wavelength of the excitation laser is 531.8 nm.

wave plate and the analyzer polarizer before entering the detector. Circular polarization of the same or opposite helicity to that of the incident light is selected by setting the direction of the analyzer perpendicular or parallel to that of the incident polarizer. For convenience, we use (σ_s σ_i) = (σ+ σ+) or (σ− σ−) for helicity-conserved Raman scattering and (σ_s σ_i) = (σ+ σ−) or (σ− σ+) for helicity-changed Raman scattering, respectively.

Vertical graphene (VG) arrays were grown via an alcohol-based electric-assisted plasma-enhanced chemical vapor deposition (AEF-PECVD) method onto the Si/SiO_2 substrate.[15] Figure 1b,d shows the cross-sectional SEM images of a VG array and a randomly oriented graphene array, respectively. The graphene flakes of the VG array are almost vertical to the substrate as in Figure 1b, while the orientations of graphene sheets are disorganized as shown in Figure 1d. The corresponding helicity-resolved Raman spectra of the two graphene arrays excited by a 531.8 nm laser are shown in Figure 1c,e. The intensity of the G mode at 1584 cm^{-1} under (σ+ σ−) configuration is significantly higher than that under (σ+ σ+) for the randomly oriented graphene array (Figure 1e). However, the intensities are almost identical for the VG array (Figure 1c). It should be noted that the intensity of the 2D mode at 2696 cm^{-1} under (σ+ σ+) configuration is almost the same as that under (σ+ σ−) configuration for both the VG array and the randomly oriented array (see the Supporting Information, S1). This is further proved by the same intensities of the 2D mode under (σ+ σ+) and (σ+ σ−) configurations for graphene with other orientations (see the Supporting Information, S2). All of the Raman spectra were normalized by the intensities of the 2D band. Furthermore, when the wavelength of the excitation laser is changed to 632.8 nm, the intensity of the G mode under (σ+ σ−) is also much higher than that under (σ+ σ+) for the randomly oriented graphene array, while the intensities are almost identical for the VG array. Similarly, the intensities of the 2D mode are almost the same for the two graphene arrays (see the Supporting Information, S3). However, it is completely different when the laser is linearly polarized. For graphene arrays with different orientations, the intensities under the parallel polarization configuration are always much higher than that

https://doi.org/10.1021/acs.jpcc.1c01937
J. Phys. Chem. C 2021, 125, 8353−8359

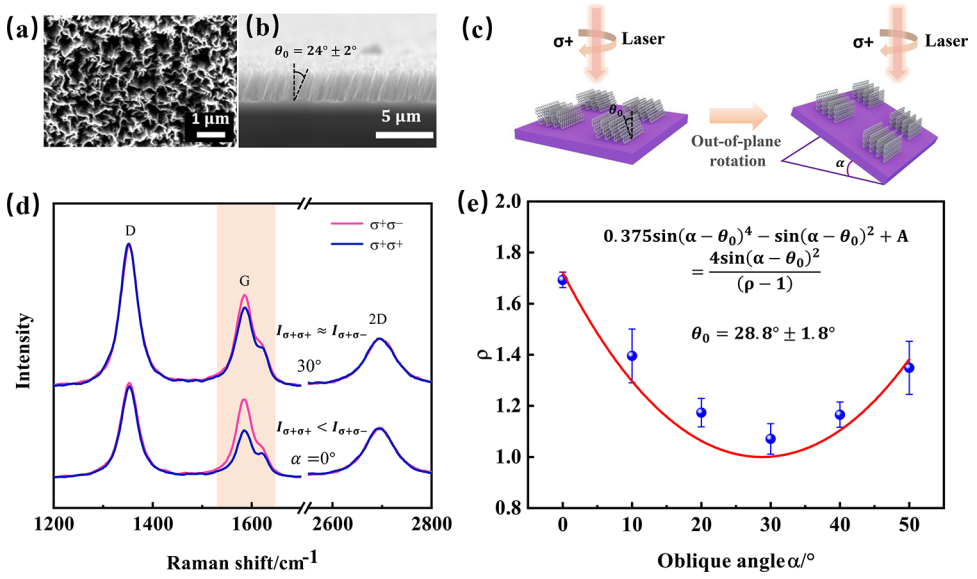

Figure 4. Determining the oblique angle of a VG array. (a, b) Top-view (a) and the cross-sectional (b) SEM images of the VG array with an oblique angle θ_0. (c) Schematic diagram of tilting the substrate with an angle α. The graphene sheets on the right part are vertical to the horizontal plane. (d) Helicity-resolved Raman spectra of the sample with tilting angles 0 and 30°. (e) Correlation of ρ for the G mode of the VG array with a tilting angle α. The formula given in the inset is used to fit the data. The Raman spectra were normalized by the intensities of the 2D band. The wavelength of the laser is 531.8 nm.

under the vertical polarization configuration for both G and 2D bands (see the Supporting Information, S4).

According to the Raman selection rules, the intensity of the Raman scattered light can be expressed by the following equation

$$I \propto |e_s \cdot R \cdot e_i|^2 \tag{1}$$

where e_i and e_s are Jones vectors and represent the polarization directions of the incident and scattering light, respectively, and R is the Raman tensor that depends on the symmetry of the crystal and the vibrational mode.[28]

The G mode intensity of a graphene sheet with orientation $(\theta,\varphi,\varepsilon)$, where the nutation angle θ (out-of-plane orientation angle), the precession angle φ (in-plane orientation angle), and the rotation angle ε are defined in Figure 2a, under $(\sigma+\ \sigma-)$ and $(\sigma+\ \sigma+)$ configurations can be calculated as (see the Supporting Information for details, S5)

$$I_{\sigma+\sigma+} \propto d^2(\cos\theta^2 - 1)^2 = d^2 \sin\theta^4 \tag{2}$$

$$I_{\sigma+\sigma-} \propto d^2(\cos\theta^2 + 1)^2 + 4d^2\cos\theta^2 \tag{3}$$

It is clearly seen that the intensities for both $(\sigma+\ \sigma-)$ and $(\sigma+\ \sigma+)$ configurations are independent of the in-plane orientation angle φ and the rotation angle ε, but depend only on the out-of-plane orientation angle θ. For a horizontal graphene sheet ($\theta = 0°$), as shown in Figure 2b, $I_{\sigma+\sigma+} = 0$ and $I_{\sigma+\sigma-} \propto 2d^2$, which means that the G band is helicity-changed Raman scattering.[36] For a vertical graphene sheet, shown in Figure 2c ($\theta = 90°$), the Raman intensities are the same for both configurations and the circular polarization ratio $\rho = \frac{I_{\sigma+\sigma-}}{I_{\sigma+\sigma+}} = 1$. Moreover, the circular polarization ratio ρ must be greater than 1 for graphene sheets with all possible orientations, except for $\theta = 0$ and 90°, and ρ increases with increase in the orientation angle θ. These explain well the experimental observations in Figure 1c,e, which show $\rho > 1$ for the randomly oriented graphene array, while $\rho \approx 1$ for the VG array.

Due to the superior heat conductivity of graphene, VG arrays have shown great potential in applications such as thermal interface materials. The oblique angle is a determinative parameter that affects the heat transfer capability. In the following, we show that the oblique angle can be measured using HRRS. For simplicity and distinction, we use α to represent the tilting angle of the VG array, while θ is used to denote the out-of-plane angle of a single graphene sheet with respect to the horizontal plane. In order to obtain an analytical model of the circular polarization ratio ρ with the tilting angle α, the VG sample was tilted from 0 to 60°, as depicted in Figure 3a. Note that the out-of-plane angle θ is different for graphene sheets with a different in-plane orientation angle φ. For example, the out-of-plane orientation angle θ of the graphene sheet M (indicated by the right arrow in Figure 3a) is always 90°, while the out-of-plane orientation angle of the graphene sheet N (indicated by the left arrow in Figure 3a) is $(90° - \alpha)$. Generally, the out-of-plane angle θ is related to α as

$$\cos\theta = \sin\varphi \sin\alpha \tag{4}$$

where φ is the in-plane angle of graphene sheets as shown in Figure 3a. Assuming that the in-plane angle φ is arbitrary for a VG array, the Raman-scattered intensity of the VG array with a tilting angle α can then be obtained by the following integrals (see the Supporting Information for details, S6)

$$\int_0^{\pi} I_{\sigma+\sigma+} d\varphi \propto \frac{3}{8}\pi \sin\alpha^4 - 2\sin\alpha^2 \cdot \frac{1}{2}\pi + A\cdot\pi \tag{5}$$

$$\int_0^{\pi} I_{\sigma+\sigma-} d\varphi \propto \frac{3}{8}\pi \sin\alpha^4 + 6\sin\alpha^2 \cdot \frac{1}{2}\pi + A\cdot\pi \tag{6}$$

where A is a constant representing equal contributions to $I_{\sigma+\sigma+}$ and $I_{\sigma+\sigma-}$ of the G mode; for example, by impurities such as amorphous carbon. The value of parameter A is 1 if the sample is a perfect VG array without any impurity, and increases with the content of impurity. Finally, the relationship between the

https://doi.org/10.1021/acs.jpcc.1c01937
J. Phys. Chem. C 2021, 125, 8353−8359

oblique angle α and the circular polarization ratio ρ of the G mode intensities can be written as

$$0.375 \sin \alpha^4 - \sin \alpha^2 + A = \frac{4 \sin \alpha^2}{(\rho - 1)} \quad (7)$$

Helicity-resolved Raman spectra of the VG array at different tilting angles (α) up to 60° were measured, and are plotted in Figure 3b. All of the Raman spectra were normalized by the intensities of the 2D band, which shows no circular polarization dependence. It is apparent that the D band intensities are also the same for both configurations. However, the intensity difference of the G band between ($\sigma+$ $\sigma-$) and ($\sigma+$ $\sigma+$) configurations becomes larger as the tilting angle increases. The circular polarization ratios are extracted and plotted in Figure 3c. The data can be well fitted using eq 7 with R^2 of 0.997, and the value of parameter A is fitted as 5.65.

In practice, the oblique angle of VG arrays can be changed by tuning PECVD parameters. Exceptional changes of the oblique angle are also possible during sample transfer and device fabrication, which affects the performance such as heat conductivity in thermal management. The above model can be used to effectively determine the oblique angle of unknown VG arrays. Figure 4a,b shows the top-view and the cross-sectional SEM images of a VG array with an oblique angle θ_0, which was measured to be 24 ± 2°.

In order to determine the oblique angle θ_0 using HRRS, the VG array is tilted by an angle α, as shown in Figure 4c. According to eqs 5 and 6, the oblique angle θ_0 can be obtained by changing α until $I_{\sigma+\sigma+} = I_{\sigma+\sigma-}$ is satisfied, or the least polarization ratio is found (Figure 4d). The oblique angle can also be determined more accurately by fitting the α-dependent circular polarization ratios (Figure 4e) using the following equation

$$0.375 \sin(\alpha - \theta_0)^4 - \sin(\alpha - \theta_0)^2 + A = \frac{4 \sin(\alpha - \theta_0)^2}{(\rho - 1)} \quad (8)$$

From curve fitting, the oblique angle $\theta_0 = 28.8 \pm 1.8°$ and $A = 1.49$ are obtained. The value of the angle matches well with that measured by SEM with an error of less than 5°, which implies that our approach is highly reliable and accurate. In comparison to the commonly used methods, such as cross-sectional SEM, our method is noninvasive and can be used for in situ measurements of devices. In principle, our method can also be extended to measure various assemblies of nanomaterials such as vertical arrays of different 2D materials or carbon nanotubes, and kinds of polymer nanocomposites reinforced with graphene or carbon nanotubes.

CONCLUSIONS

The microscopic structure of nanomaterials assembly determines the performance in practical functional applications. Raman spectroscopy stands out as one of the most popular tools for structure characterization and, particularly, the orientation of nanomaterial assemblies. We proposed a technique of helicity-resolved Raman spectroscopy (HRRS) to determine the oblique angle of VG arrays, which is crucial for thermal management applications. Due to the nature of circular polarization, the in-plane orientation angle φ has no influence on the intensity of the G mode, which greatly simplified the theoretical model. We showed that the oblique angle of VG arrays can be measured through the circular polarization ratio ρ of the G mode intensity for ($\sigma+$ $\sigma-$) and ($\sigma+$ $\sigma+$) configurations. The oblique angle of a VG array was determined quantitatively by tilting the substrate with an error of less than 5°, which implies that our technique is highly reliable and accurate. The model we proposed can be extended to determine the out-of-plane orientation of other materials such as vertical carbon nanotube arrays or carbon nanotube fibers. In principle, if we combined linearly polarized Raman spectroscopy and HRRS, three-dimensional spatial orientations of various nanomaterial assemblies can be well characterized.

ASSOCIATED CONTENT

Supporting Information

The Supporting Information is available free of charge at https://pubs.acs.org/doi/10.1021/acs.jpcc.1c01937.

Helicity-resolved Raman spectra of the VG array and the randomly oriented graphene array without normalization for 531.8 nm excitation wavelength; helicity-resolved Raman spectra of the 2D mode for graphene with tiling angles from 0 to 50°; helicity-resolved Raman spectra of the VG array, the VG array with an oblique angle 24°, and the randomly oriented graphene array for 632.8 nm excitation wavelength; linearly polarized Raman spectra of the VG array, the VG array with an oblique angle 24°, and the randomly oriented graphene array under parallel and perpendicular configurations; calculation of Raman scattered intensities for a graphene sheet with different orientation angles; and calculation of Raman scattered intensities for VG arrays with different tilting angles (PDF)

AUTHOR INFORMATION

Corresponding Author

Lianming Tong − *Center for Nanochemistry, Beijing Science and Engineering Center for Nanocarbons, Beijing National Laboratory for Molecular Sciences, College of Chemistry and Molecular Engineering, Peking University, Beijing 100871, P. R. China;* orcid.org/0000-0001-7771-4077; Email: tonglm@pku.edu.cn

Authors

Bo Xu − *Academy for Advanced Interdisciplinary Studies, Peking University, Beijing 100871, P. R. China; Center for Nanochemistry, Beijing Science and Engineering Center for Nanocarbons, Beijing National Laboratory for Molecular Sciences, College of Chemistry and Molecular Engineering, Peking University, Beijing 100871, P. R. China*

Shichen Xu − *Center for Nanochemistry, Beijing Science and Engineering Center for Nanocarbons, Beijing National Laboratory for Molecular Sciences, College of Chemistry and Molecular Engineering, Peking University, Beijing 100871, P. R. China*

Yan Zhao − *Academy for Advanced Interdisciplinary Studies, Peking University, Beijing 100871, P. R. China; Center for Nanochemistry, Beijing Science and Engineering Center for Nanocarbons, Beijing National Laboratory for Molecular Sciences, College of Chemistry and Molecular Engineering, Peking University, Beijing 100871, P. R. China*

Shishu Zhang − *Center for Nanochemistry, Beijing Science and Engineering Center for Nanocarbons, Beijing National Laboratory for Molecular Sciences, College of Chemistry and*

https://doi.org/10.1021/acs.jpcc.1c01937
J. Phys. Chem. C 2021, 125, 8353−8359

Molecular Engineering, Peking University, Beijing 100871, P. R. China

Rui Feng − *Academy for Advanced Interdisciplinary Studies, Peking University, Beijing 100871, P. R. China; Center for Nanochemistry, Beijing Science and Engineering Center for Nanocarbons, Beijing National Laboratory for Molecular Sciences, College of Chemistry and Molecular Engineering, Peking University, Beijing 100871, P. R. China*

Jin Zhang − *Center for Nanochemistry, Beijing Science and Engineering Center for Nanocarbons, Beijing National Laboratory for Molecular Sciences, College of Chemistry and Molecular Engineering, Peking University, Beijing 100871, P. R. China;* orcid.org/0000-0003-3731-8859

Complete contact information is available at: https://pubs.acs.org/10.1021/acs.jpcc.1c01937

Author Contributions

B.X. conceived the idea and designed the experiments. S.X. provided the AEF-PECVD grown vertical graphene arrays. B.X. and L.T. wrote the manuscript. The work was supervised by L.T. and J.Z. All the authors discussed the results and commented on the manuscript.

Notes

The authors declare no competing financial interest.

■ ACKNOWLEDGMENTS

This work was financially supported by the Ministry of Science and Technology of China (2016YFA0200100 and 2018YFA0703502), the National Natural Science Foundation of China (Grant Nos. 52021006, 51720105003, 21790052, 21974004), the Strategic Priority Research Program of CAS (XDB36030100), and the Beijing National Laboratory for Molecular Sciences (BNLMS-CXTD-202001).

■ REFERENCES

(1) Xu, S.; Zhang, J. Vertically Aligned Graphene for Thermal Interface Materials. *Small Struct.* **2020**, *1*, No. 2000034.

(2) Liu, C.; Kong, D.; Hsu, P. C.; Yuan, H.; Lee, H. W.; Liu, Y.; Wang, H.; Wang, S.; Yan, K.; Lin, D.; et al. Rapid Water Disinfection Using Vertically Aligned MoS_2 Nanofilms and Visible Light. *Nat. Nanotechnol.* **2016**, *11*, 1098−1104.

(3) Biercuk, M. J.; Llaguno, M. C.; Radosavljevic, M.; Hyun, J. K.; Johnson, A. T.; Fischer, J. E. Carbon Nanotube Composites for Thermal Management. *Appl. Phys. Lett.* **2002**, *80*, 2767−2769.

(4) Xie, D.; Xia, X. H.; Zhong, Y.; Wang, Y. D.; Wang, D. H.; Wang, X. L.; Tu, J. P. Exploring Advanced Sandwiched Arrays by Vertical Graphene and N-Doped Carbon for Enhanced Sodium Storage. *Adv. Energy Mater.* **2017**, *7*, No. 1601804.

(5) Barth, J. V.; Costantini, G.; Kern, K. Engineering Atomic and Molecular Nanostructures at Surfaces. *Nature* **2005**, *437*, 671−679.

(6) Young, R. J.; Kinloch, I. A.; Gong, L.; Novoselov, K. S. The Mechanics of Graphene Nanocomposites: A Review. *Compos. Sci. Technol.* **2012**, *72*, 1459−1476.

(7) Coleman, J. N.; Khan, U.; Gun'ko, Y. K. Mechanical Reinforcement of Polymers Using Carbon Nanotubes. *Adv. Mater.* **2006**, *18*, 689−706.

(8) Balandin, A. A. Thermal Properties of Graphene and Nanostructured Carbon Materials. *Nat. Mater.* **2011**, *10*, 569−581.

(9) Papageorgiou, D. G.; Li, Z.; Liu, M.; Kinloch, I. A.; Young, R. J. Mechanisms of Mechanical Reinforcement by Graphene and Carbon Nanotubes in Polymer Nanocomposites. *Nanoscale* **2020**, *12*, 2228−2267.

(10) Vigolo, B.; Penicaud, A.; Coulon, C.; Sauder, C.; Pailler, R.; Journet, C.; Bernier, P.; Poulin, P. Macroscopic Fibers and Ribbons of Oriented Carbon Nanotubes. *Science* **2000**, *290*, 1331−1334.

(11) Dai, W.; Ma, T. F.; Yan, Q. W.; Gao, J. Y.; Tan, X.; Lv, L.; Hou, H.; Wei, Q. P.; Yu, J. H.; Wu, J. B.; Maruyama, S.; Lin, C. T.; et al. Metal-Level Thermally Conductive yet Soft Graphene Thermal Interface Materials. *ACS Nano* **2019**, *13*, 11561−11571.

(12) Kimura, T.; Ago, H.; Tobita, M.; Ohshima, S.; Kyotani, M.; Yumura, M. Polymer Composites of Carbon Nanotubes Aligned by a Magnetic Field. *Adv. Mater.* **2002**, *14*, 1380−1383.

(13) Ajayan, P. M.; Stephan, O.; Colliex, C.; Trauth, D. Aligned Carbon Nanotube Arrays Formed by Cutting a Polymer Resin-Nanotube Composite. *Science* **1994**, *265*, 1212−1214.

(14) Yang, Y.; Li, X. J.; Chu, M.; Sun, H. F.; Jin, J.; Yu, K. H.; Wang, Q. M.; Zhou, Q. F.; Chen, Y. Electrically Assisted 3D Printing of Nacre-Inspired Structures with Self-Sensing Capability. *Sci. Adv.* **2019**, *5*, No. eaau9490.

(15) Xu, S.; Wang, S.; Chen, Z.; Sun, Y.; Gao, Z.; Zhang, H.; Zhang, J. Electric-Field-Assisted Growth of Vertical Graphene Arrays and the Application in Thermal Interface Materials. *Adv. Funct. Mater.* **2020**, *30*, No. 2203302.

(16) Xin, G. Q.; Yao, T. K.; Sun, H. T.; Scott, S. M.; Shao, D. L.; Wang, G. K.; Lian, J. Highly Thermally Conductive and Mechanically Strong Graphene Fibers. *Science* **2015**, *349*, 1083−1087.

(17) Chae, H. G.; Sreekumar, T. V.; Uchida, T.; Kumar, S. A Comparison of Reinforcement Efficiency of Various Types of Carbon Nanotubes in Poly Acrylonitrile Fiber. *Polymer* **2005**, *46*, 10925−10935.

(18) Lin, X. Y.; Shen, X.; Zheng, Q. B.; Yousefi, N.; Ye, L.; Mai, Y. W.; Kim, J. K. Fabrication of Highly-Aligned, Conductive, and Strong Graphene Papers Using Ultralarge Graphene Oxide Sheets. *ACS Nano* **2012**, *6*, 10708−10719.

(19) Mignuzzi, S.; Pollard, A. J.; Bonini, N.; Brennan, B.; Gilmore, I. S.; Pimenta, M. A.; Richards, D.; Roy, D. Effect of Disorder on Raman Scattering of Single-Layer MoS_2. *Phys. Rev. B* **2015**, *91*, No. 195411.

(20) Das, A.; Pisana, S.; Chakraborty, B.; Piscanec, S.; Saha, S. K.; Waghmare, U. V.; Novoselov, K. S.; Krishnamurthy, H. R.; Geim, A. K.; Ferrari, A. C.; et al. Monitoring Dopants by Raman Scattering in an Electrochemically Top-Gated Graphene Transistor. *Nat. Nanotechnol.* **2008**, *3*, 210−215.

(21) Zhang, M.; Wu, J. X.; Zhu, Y. M.; Dumcenco, D. O.; Hong, J. H.; Mao, N. N.; Deng, S. B.; Chen, Y. F.; Yang, Y. L.; Jin, C. H.; et al. Two-Dimensional Molybdenum Tungsten Diselenide Alloys: Photoluminescence, Raman Scattering, and Electrical Transport. *ACS Nano* **2014**, *8*, 7130−7137.

(22) Damen, T. C.; Porto, S. P. S.; Tell, B. Raman Effect in Zinc Oxide. *Phys. Rev.* **1966**, *142*, 570−574.

(23) Rousseau, D. L.; Bauman, R. P.; Porto, S. P. S. Normal Mode Determination in Crystals. *J. Raman Spectrosc.* **1981**, *10*, 253−290.

(24) Steele, J. A.; Puech, P.; Lewis, R. A. Polarized Raman Backscattering Selection Rules for (hhl)-Oriented Diamond- and Zincblende-Type Crystals. *J. Appl. Phys.* **2016**, *120*, No. 055701.

(25) Sanson, A.; Giarola, M.; Bettinelli, M.; Speghini, A.; Mariotto, G. Polarized Micro-Raman Spectroscopy and ab Initio Phonon Modes Calculations of $LuPO_4$. *J. Raman Spectrosc.* **2013**, *44*, 1411−1415.

(26) Šubr, M.; Prochazka, M. Polarization- and Angular-Resolved Optical Response of Molecules on Anisotropic Plasmonic Nanostructures. *Nanomaterials* **2018**, *8*, No. 418.

(27) Zhang, S. S.; Zhang, N.; Zhao, Y.; Cheng, T.; Li, X. B.; Feng, R.; Xu, H.; Liu, Z. R.; Zhang, J.; Tong, L. M. Spotting the Differences in Two-Dimensional Materials - the Raman Scattering Perspective. *Chem. Soc. Rev.* **2018**, *47*, 3217−3240.

(28) Loudon, R. Raman Effect in Crystals. *Adv. Phys.* **2001**, *50*, 813−864.

(29) Liu, T.; Kumar, S. Quantitative Characterization of SWNT Orientation by Polarized Raman Spectroscopy. *Chem. Phys. Lett.* **2003**, *378*, 257−262.

(30) Tanaka, M.; Young, R. J. Polarised Raman Spectroscopy for the Study of Molecular Orientation Distributions in Polymers. *J. Mater. Sci.* **2006**, *41*, 963−991.

(31) Wu, J. X.; Mao, N. N.; Xie, L. M.; Xu, H.; Zhang, J. Identifying the Crystalline Orientation of Black Phosphorus Using Angle-Resolved Polarized Raman Spectroscopy. *Angew. Chem., Int. Ed.* **2015**, *54*, 2366−2369.
(32) Chenet, D. A.; Aslan, O. B.; Huang, P. Y.; Fan, C.; van der Zande, A. M.; Heinz, T. F.; Hone, J. C. In-Plane Anisotropy in Mono- and Few-Layer ReS_2 Probed by Raman Spectroscopy and Scanning Transmission Electron Microscopy. *Nano Lett.* **2015**, *15*, 5667−5672.
(33) Zhang, S. S.; Mao, N. N.; Zhang, N.; Wu, J. X.; Tong, L. M.; Zhang, J. Anomalous Polarized Raman Scattering and Large Circular Intensity Differential in Layered Triclinic Res2. *ACS Nano* **2017**, *11*, 10366−10372.
(34) Song, Q. J.; Pan, X. C.; Wang, H. F.; Zhang, K.; Tan, Q. H.; Li, P.; Wan, Y.; Wang, Y. L.; Xu, X. L.; Lin, M. L.; et al. The in-Plane Anisotropy of WTe_2 Investigated by Angle-Dependent and Polarized Raman Spectroscopy. *Sci. Rep.* **2016**, *6*, No. 29254.
(35) Tatsumi, Y.; Kaneko, T.; Saito, R. Conservation Law of Angular Momentum in Helicity-Dependent Raman and Rayleigh Scattering. *Phys. Rev. B* **2018**, *97*, No. 195444.
(36) Tatsumi, Y.; Saito, R. Interplay of Valley Selection and Helicity Exchange of Light in Raman Scattering for Graphene and MoS_2. *Phys. Rev. B* **2018**, *97*, No. 115407.
(37) Zhao, Y.; Zhang, S.; Shi, Y.; Zhang, Y.; Saito, R.; Zhang, J.; Tong, L. Characterization of Excitonic Nature in Raman Spectra Using Circularly Polarized Light. *ACS Nano* **2020**, *14*, 10527−10535.
(38) Zhao, Y.; Han, S.; Zhang, J.; Tong, L. Helicity-Resolved Resonant Raman Spectroscopy of Layered WS_2. *J. Raman Spectrosc.* **2021**, *52*, 525−531.
(39) Chen, S. Y.; Zheng, C. X.; Fuhrer, M. S.; Yan, J. Helicity-Resolved Raman Scattering of MoS_2, $MoSe_2$, WS_2, and WSe_2 Atomic Layers. *Nano Lett.* **2015**, *15*, 2526−2532.
(40) Zhao, Y.; Sun, Y.; Bai, M.; Xu, S.; Wu, H.; Han, J.; Yin, H.; Guo, C.; Chen, Q.; Chai, Y.; et al. Raman Spectroscopy of Dispersive Two-Dimensional Materials: A Systematic Study on MoS_2 Solution. *J. Phys. Chem. C* **2020**, *124*, 11092−11099.

https://doi.org/10.1021/acs.jpcc.1c01937
J. Phys. Chem. C 2021, 125, 8353−8359